Attosecond Shock Waves

P. A. Zhokhov[1,2] and A. M. Zheltikov[1,2,3]

[1]Department of Physics and Astronomy, Texas A&M University, College Station, Texas 77843, USA
[2]Russian Quantum Center, 143025 Skolkovo, Moscow Region, Russia
[3]Physics Department, International Laser Center, M.V. Lomonosov Moscow State University, 119992 Moscow, Russia

(Received 18 October 2012; published 3 May 2013)

Shock-wave formation is a generic scenario of wave dynamics known in nonlinear acoustics, fluid dynamics, astrophysics, seismology, and detonation physics. Here, we show that, in nonlinear optics, remarkably short, attosecond shock transients can be generated through a strongly coupled spatial and temporal dynamics of ultrashort light pulses, suggesting a pulse self-compression scenario whereby multigigawatt attosecond optical waveforms can be synthesized.

DOI: 10.1103/PhysRevLett.110.183903 PACS numbers: 42.65.Sf

A shock wave is a generic term for an abrupt, often discontinuous, transient disturbance of physical parameters that exhibits a clearly pronounced wavelike behavior as it propagates through a medium [1–3]. Examples of shock waves are found in fluid dynamics, nonlinear acoustics, astrophysics, seismology, and detonation physics and include such diversified natural phenomena as thunder, volcanic and stellar explosions, earthquakes, and tsunamis [4]. An important class of shock waves, observed in ocean physics, acoustics, and nonlinear electrodynamics, is produced through a nonlinear wave steepening. In optics, this type of nonlinearity translates into the intensity dependence of the group velocity, leading to a self-steepening of one of the pulse edges. Following the early theoretical predictions in the 1960s [5], optical shock waves have been experimentally demonstrated [6,7] and insightfully explained [8] in terms of the nonlinear wave-evolution equation as a part of the classical work on spectral broadening of ultrashort laser pulses in nonlinear media. In more recent studies, shock-wave effects have been shown to play an important role in supercontinuum generation in highly nonlinear fibers [9,10], as well as in ultrafast optical waveform dynamics in laser-induced filaments [11–14].

One-dimensional shock-wave effects, observed in optical fibers [15], are known to steepen the trailing edge of the pulse but do not lead to pulse shortening. Similar to hydrodynamic shocks, which obey a set of well-defined conservation and propagation laws [16], 1D shock waves in nonlinear optics have been shown to satisfy energy and photon-number conservation [17–19] and to evolve in accordance with fundamental equations of electrodynamics [15], allowing in some approximations compact analytical self-similar solutions.

Here, we demonstrate that a three-dimensional dynamics of ultrashort light pulses, which involves strongly coupled spatial and temporal nonlinear effects, can give rise to isolated optical shock transients with remarkably short, subfemtosecond pulse widths, suggesting an ionization-free pulse self-compression scenario whereby multigigawatt attosecond optical waveforms can be synthesized.

In our analysis, we use the generalized nonlinear Schrödinger equation for the field envelope $A \equiv A(t, r, z)$, modified to include ionization effects [11,12,20]:

$$\frac{\partial A}{\partial z} = iT^{-1}\frac{\nabla_r^2 A}{2k_0} + \mathcal{R}_i[A] + iD(\omega)A + iT\frac{\omega_0}{c}(n_2|A|^2 A + \chi_{TH}A^3 e^{-2i\omega_0 t} + n_4|A|^4 A). \quad (1)$$

Here r is the radial coordinate, $\nabla_r^2 = (1/r)(\partial/\partial r)r(\partial/\partial r)$ is the transverse Laplacian, z is the propagation coordinate, $k(\omega) = (\omega/c)n(\omega)$, ω is the radiation frequency, $n(\omega)$ is the frequency-dependent linear refractive index, $T = 1 + (i/\omega_0)(\partial/\partial t)$ is the self-steepening operator, t is the retarded time, ω_0 is the central frequency of the pulse, n_2 and n_4 are the coefficients in the power-series expansion of the refractive index in the field intensity, $\chi_{TH} = (\omega/ck(\omega))\sqrt{(\mu_0/\epsilon_0)}\chi^{(3)}(3\omega; \omega, \omega, \omega)$, $\chi^{(3)}(3\omega; \omega, \omega, \omega)$ is the nonlinear susceptibility responsible for third-harmonic generation, and $D(\omega) = k(\omega) - (\omega/V)$ is the dispersion operator, $V = [\partial k(\omega)/\partial\omega]_{\omega_0}^{-1}$ being the group velocity.

Ionization effects are included through the $\mathcal{R}_i[A]$ term:

$$\mathcal{R}_i = -\mathcal{F}^{-1}\left[\frac{\sigma(\omega)(1 + i\omega\tau_c)}{2}\mathcal{F}[N_e A]\right] - U_i\frac{N_{at}W(|A|^2)}{|A|^2}, \quad (2)$$

where $\mathcal{F}$ is the Fourier transform from t to ω, $\mathcal{F}^{-1}$ is the inverse Fourier transform, $\sigma(\omega) = (\mu_0 e^2\omega\tau_c)/(mk(\omega) \times (1 + \omega^2\tau_c^2))$ is the inverse bremsstrahlung cross section, e is the electron charge, m is the electron mass, μ_0 is the vacuum permeability, τ_c is the electron momentum transfer time, N_{at} is the atomic density, $W(|A|^2)$ is the single-atom photoionization rate, and U_i is the ionization potential. The electron density $N_e \equiv N_e(t, r, z)$ is

found from the equation $(\partial N_e)/(\partial t) = N_{at}W(|A|^2) + (\sigma(\omega_0)/U_i)N_e|A|^2$, which accounts for photoionization and impact ionization.

To identify the scaling laws behind the dynamics of ultrashort optical waveforms, we use the dimensionless time and space variables $\tau = \omega_0 t$, $\Omega = \omega/\omega_0$, $\rho = r/a$, and $\eta = z/L_d$, where a is the initial beam radius, $L_d = (\omega_0 a^2/2c)n_0$ is the diffraction length, and $n_0 = n(\omega_0)$ to represent Eq. (1) in the following dimensionless form:

$$\frac{\partial \mathcal{A}}{\partial \eta} = iT^{-1}\frac{\nabla_\rho^2 \mathcal{A}}{4} + iT(|\mathcal{A}|^2\mathcal{A} + \phi\mathcal{A}^3 e^{-2i\tau} + \mu|A|^4 A) + D(\omega_0\Omega)\mathcal{A} - i\xi T^{-1}\int_{-\infty}^{\tau} \mathcal{W}(|\mathcal{A}|^2)d\tau'\mathcal{A} - \theta\frac{\mathcal{W}(|\mathcal{A}|^2)}{|\mathcal{A}|^2}. \quad (3)$$

Here, $\mathcal{A} = \sqrt{(\pi a^2/P_{cr})}A$ is the dimensionless field amplitude, $\phi = \chi_{TH}/n_2$, $\mu = (n_4/n_2)(P_{cr}/\pi a^2)$, $\xi = L_d/L_i$, $L_i = [(\omega_0/c)(N_{at}/2N_{cr})]^{-1}$ is the ionization length, $N_{cr} = (\omega_0^2\epsilon_0 m)/e^2$ is the critical plasma density, N_{at} is the density of the gas atoms, $\theta = L_d/L_{PA}$, $L_{PA} = [(\pi a^2/P_{cr})(U_i/2)N_{at}\omega_0]^{-1}$ is the photoabsorption length, and $\mathcal{W}(|\mathcal{A}|^2) = \omega_0^{-1}W((P_{cr}/\pi a^2)|\mathcal{A}|^2)$. Deriving Eq. (3), we do the standard assumption that the impact ionization is negligible, since pulse duration is much shorter than the electron momentum transfer time τ_c.

The input peak power in our simulations was chosen slightly below the critical power of self-focusing $P_{cr} = \lambda_0^2/(2\pi n_0 n_2)$, where $\lambda_0 = 2\pi c/\omega_0$ is the central wavelength and n_0 is the linear field-free refractive index. The initial beam sizes and the focusing geometry were varied in a broad range to achieve a specific scenario of space-time self-focusing where the self-steepening of the trailing edge of the pulse is accompanied by the diffraction of the leading edge of the pulse, allowing a shock wave to evolve toward an extremely short pulse width.

Equations (1)–(3) are integrated numerically by using the split-step method [21]. The linear parts of Eqs. (1)–(3) are simulated by using the Hankel transform [22] in the radial coordinate. The nonlinear parts in these equations are computed by using the fourth-order Runge-Kutta procedure. The computational grid is uniform along t with a step $\Delta t = 41$ as and $\Delta\tau = 0.1$. The grid along the radial coordinate consists of 2048 points at the nodes of the first-order Bessel function, with the radial coordinate varied from 3.7 μm to 1 cm. The step size along z is adjusted so that the nonlinear phase shift at each step does not exceed 0.01 rad. The equation for the electron density is integrated by using the Heun scheme of the second-order Runge-Kutta method.

Helium was chosen as a nonlinear medium in our simulations because of its high ionization potential ($U_i \approx$ 24.59 eV), providing a broad transparency range, needed to support the spectrum of subfemtosecond shock-wave transients. The nonlinear refractive indices for helium are $n_2 \approx 3 \times 10^{-8}(p/p_0)$ cm^2/TW and $n_4 \approx -1 \times 10^{-11}(p/p_0)$ cm^4/TW^2 [23–26], where p is the gas pressure and p_0 is the atmospheric pressure. The entire dispersion profile of the gas is included in the model through the $n(\omega)$ data for helium from Ref. [27]. The third-harmonic term in Eqs. (1)–(3) may have a detectable influence on the shape of ultrashort shock transients studied in this work but does not lead to dramatic changes in the scenario of shock-wave generation and is omitted from the numerical analysis presented below. Third-harmonic generation and other physical effects and factors that may influence this scenario will be considered in greater detail in a follow-up publication.

Laser pulses with a peak power well above P_{cr} tend to form filaments in accordance with the standard filamentation scenario as beam self-focusing due to the Kerr nonlinearity of the gas is balanced by ionization-induced defocusing. As shown by the extensive earlier work (see, e.g., Refs. [11,12] for review), this regime of beam dynamics, accurately reproduced in our simulations, enables pulse compression to few-cycle pulse widths. A drastically different scenario of field evolution is observed for loosely focused laser beams with peak powers slightly below P_{cr}. This regime of nonlinear spatiotemporal field dynamics is illustrated in Fig. 1(a) for an input field with a peak power $P = 0.8P_{cr}$ taken in the form of Gaussian pulse with dimensionless pulse width $\tau_0 = 70$ and Gaussian spatial profile, focused in helium with a focal length $f = 0.65L_d$. An ultrashort shock wave is seen to build up on the trailing edge of the pulse [Fig. 1(a)] as a result of this spatiotemporal field evolution. The minimum pulse width of this shock transient, achieved at $z = 1.1L_d$, is 1.36 fs. The beam focusing geometry in these simulations is adjusted in such a way as to enhance pulse compression and to avoid any noticeable ionization effects. Comparison of the simulations performed by using the full model of Eqs. (1)–(3) [filled circles in Fig. 1(b)] with simulations where ionization, high-order nonlinearity and ionization, or dispersion effects were switched off [open circles, triangles, and

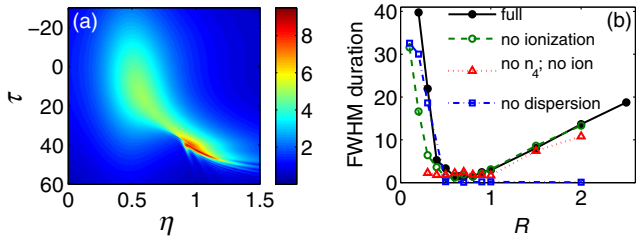

FIG. 1 (color online). (a) Spatiotemporal map of the on-axis field amplitude $\mathcal{A}$ for $f = 0.65L_d$ and (b) the minimum dimensionless FWHM pulse width on the beam axis as a function of $R = f/L_d$ calculated with the full model (solid line, filled circles), with ionization switched off (dashed line, open circles), with ionization and high-order nonlinearity switched off (dotted line, triangles), and with dispersion switched off (dash-dotted line, rectangles) for $P = 0.8P_{cr}$, $\tau_0 = 70$.

rectangles in Fig. 1(b)] shows that the minimum pulse width of the shock transient, arising on the trailing edge of the pulse, is controlled by the tradeoff of the effects related to dispersion, high-order nonlinearities, and, to some extent, ionization. For tightly focused beams [small R in Fig. 1(b)], high-order nonlinearities and ionization effects limit the pulse width. In the regime of loose focusing large R in Fig. 1(b), dispersion effects start to play a significant role, limiting the minimum pulse width of the shock transient.

When the effects of impact ionization are negligible (which is the case within a broad range of parameters, including the regime considered here), the spatiotemporal field dynamics leading to the generation of ultrashort optical shocks can be scaled in the peak power through a coordinated adjustment of the gas pressure $p \propto P^{-1}$, the input beam diameter $d_0 \propto P^{1/2}$, and the focal length $f \propto P$. As a specific example of high-power attosecond shock generation, we consider the evolution of laser pulses with a central wavelength $\lambda_0 = 800$ nm and an input pulse width of 30 fs ($\tau_0 = 70$), corresponding to a typical output of mode-locked Ti:sapphire lasers. The input pulse energies are set equal to 43 and 50 mJ, corresponding to input peak powers P_0 of 1.36 and 1.7 TW, respectively, at a helium pressure $p = 0.02$ bar. With the input beam diameter and the linear focal length taken equal to $d_0 = 2.9$ mm and $f = 15.5$ m, the maximum electron density generated by the laser pulse is 5×10^{13} cm^{-3}, and the longitudinal profiles of the field intensity and electron density along the beam path [Fig. 2(a)] drastically differ from typical field intensity and electron density profiles with extended plateaus observed in the filamentation regime [11,12].

To isolate the shock-wave effects in the generation of an ultrashort peak on the trailing edge of the pulse, seen in Figs. 3(a), 3(b), and 4(a), we performed simulations with the shock operator T in Eqs. (1) and (3) replaced by the identity operator. With the shock-wave effects switched off, a drastically different type of field evolution is observed [Figs. 3(c) and 3(d)]. For peak powers below P_{cr} [$P = 0.8P_{cr}$ in Fig. 3(c)], the pulse retains its symmetric shape, as the peak of the pulse propagates with the same group velocity as its edges. As the peak power approaches P_{cr}, ionization effects become noticeable, defocusing the trailing edge of the pulse [Fig. 3(d)]. Generation of an ultrashort pulse is not observed in any of these regimes when the shock term is disabled.

The shock term, as can be seen from Figs. 3(a)–3(d), tends to push the most intense part of the pulse toward its trailing edge, giving rise to subfemtosecond shock transients on the back of the pulse [seen at $15 < t < 20$ fs in Figs. 3(a) and 3(b)]. The physics behind shock-wave formation in this regime is intuitively clear, as the highest-intensity fraction of the pulse propagates slower than its edges due to the positive Kerr-effect-induced change in the group index of the gas. Unlike 1D shock waves, 3D shock transients can evolve toward much shorter, attosecond pulse widths due to a strongly coupled dynamics of the optical field in space and time. Specifically, in the regime illustrated by Fig. 3(a), a shock wave tends to increase the field intensity on the trailing edge of the pulse, enhancing the self-focusing of this portion of the waveform (Fig. 5). Since the field intensity on the leading edge of the pulse is much lower, this part of the pulse undergoes strong diffraction, facilitating the generation of an ultrashort shock transient. Enhancement of pulse compression due to self-steepening on the trailing edge of the pulse is confirmed by numerical simulations performed with and without the shock-wave term in Eqs. (1) and (3) (Fig. 5). At the point of maximum pulse compression [$z = 26$ m in Fig. 3(a)], an ultrashort shock is tightly confined to the pulse section where the beam size is minimal due to the most efficient self-focusing.

The field waveform produced as a result of this spatiotemporal field dynamics features an extremely short peak on a long pedestal [Fig. 4(a)]. The spectrum of this pedestal

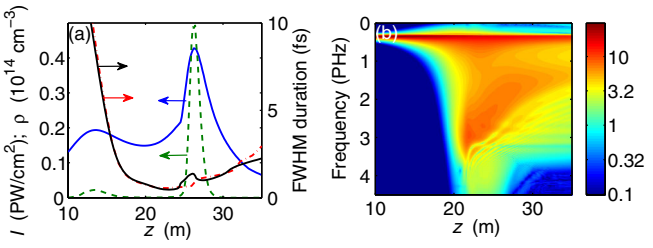

FIG. 2 (color online). (a) The maximum field intensity (solid line, left axis), the maximum electron density (dashed line, left axis), the on-axis FWHM pulse width after spectral filtering (solid line, right axis), and FWHM pulse width of the spectrally filtered field integrated over the beam (dash-dotted line, right axis) as functions of the propagation distance z and (b) the field spectrum on the beam axis for $\lambda_0 = 800$ nm, $\tau_p = 30$ fs, $f = 0.65L_d$, and $P_0 = 0.8P_{cr}$ in helium at $p = 0.02$ bar.

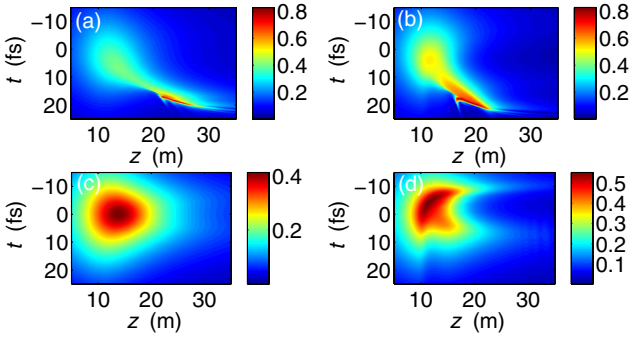

FIG. 3 (color online). Spatiotemporal maps of the on-axis field (in GV/cm), calculated with (a), (b) and without (c), (d) the shock term in Eq. (1) for the initial central wavelength $\lambda_0 = 800$ nm, input pulse width $\tau_p = 30$ fs, $f = 0.65L_d$, and input peak power $P_0 = 0.8P_{cr}$ (a), (c) and $P_0 = P_{cr}$ (b), (d) in helium with $p = 0.02$ bar.

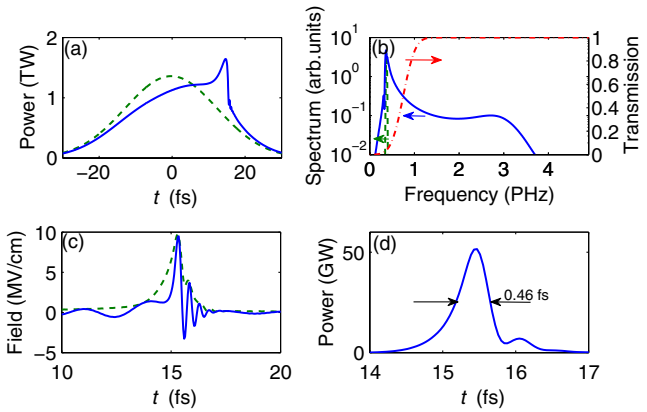

FIG. 4 (color online). (a), (b) The pulse power integrated over the entire beam and the spectrum of the pulse on the beam axis at $z = 0$ (dashed line, left axis) and 20 m (solid line, left axis). Also shown is the transmission of the filter (dotted line, right axis). (c) The electric field on the beam axis (solid line) and the pulse envelope (dashed line) at $z = 20$ m; (d) the pulse envelope integrated over the entire beam behind the filter for $\lambda_0 = 800$ nm, $\tau_p = 30$ fs, $f = 0.65L_d$, and $P_0 = 0.8P_{cr}$ in helium at $p = 0.02$ bar.

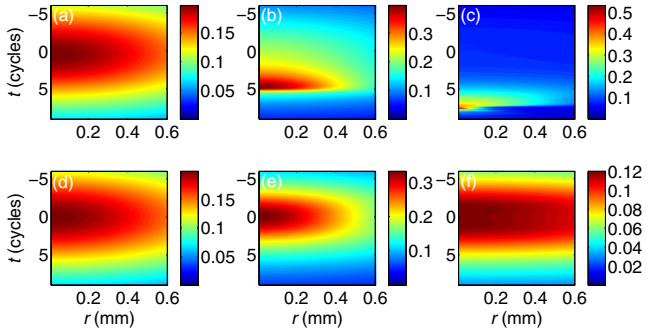

FIG. 5 (color online). Maps of the intensity (PW/cm^2) in the (r, t) coordinates simulated with (a)–(c) and without (d)–(f) the shock-wave term for (a), (d) $z = 10$ m, (b), (e) $z = 16$ m, and (c), (f) $z = 22$ for $\tau_p = 30$ fs, $P_0 = 0.8P_{cr}$, $f = 0.65L_D$, $p = 0.02$ bar.

is centered around the input spectrum [shown by the dashed line in Fig. 4(b)], while its temporal power profile follows the input pulse [the dashed line in Fig. 4(a)] slightly distorted by the shock wave. The spectrum of the ultrashort peak at $15 < t < 20$ fs in Fig. 3(a) displays a strong blueshift [Figs. 2(b) and 4(b)], translating into a strong chirp of the electric field on the beam axis [Fig. 4(c)]. Because of this spectral shift, the ultrashort shock wave can be separated from the pedestal through spectral filtering. In contrast to filamentation compression schemes, where the laser fluences are prohibitively high for a direct intrafilament filtering of the compressed pulse, the laser fluence around the point of maximum pulse compression in our scheme is below 2 J/cm^2, which allows a spectral filter to be inserted in the laser beam at $z = 21$ m to block the spectrum of the pedestal [as shown by the dash-dotted line in Fig. 4(b)] and to produce an extremely short shock transient across the entire beam with the FWHM pulse width estimated, following the integration over the beam, as 460 as. The maximum field intensity in this 0.46-fs pulse is about 2×10^3 times higher than the intensity of a prepulse 15 fs before the peak and 1.6×10^4 times higher than the postpulse intensity 15 fs after the peak. The total energy carried by this 0.46-fs shock wave is 0.03 mJ, translating into a peak power of 52 GW. The FWHM pulse width in the spectrally filtered shock wave calculated as a function of the propagation path is shown in Fig. 2(a). The integral pulse width of the compressed shock transient across the entire beam [dash-dotted curve in Fig. 2(a)] closely follows the on-axis pulse width, shown by the solid line in this figure. Equations (1) and (3) are still valid for such field transients, since all the necessary conditions for the applicability of these equations, $(1/|A|)|\partial A/\partial z| \ll k_0$ and $|k_0 - (\omega_0/V)| \ll k_0$, are satisfied, with $k_0 = (\omega_0/c)n(\omega_0)$ [20]. Indeed, for the regime where attosecond shock transients are generated, we have $\max\{(1/|A|)|\partial A/\partial z|\} \approx 10\,\mathrm{cm}^{-1}$ and $|k_0 - (\omega_0/V)| \approx 0.05$ cm^{-1}, while $k_0 \approx 8 \times 10^4$ cm^{-1}.

A broad transparency range free of any electronic resonances is critical for attosecond shock wave generation, as it helps reduce absorption, dispersion-induced pulse stretching, and precursor formation [28]. For helium, the first electronic resonance corresponds to the $1s - 2p$ transition and occurs at $\nu_{1s-2p} \approx 5.13$ PHz. For the attosecond shock transient in Fig. 4(d), the high-frequency part of the spectrum falling beyond ν_{1s-2p} carries less than 10^{-11} of the total radiation energy and less than 10^{-5} of the energy of the attosecond waveform behind the spectral filter. Under these conditions, effects related to precursor formation are negligible.

Unlike laser-induced filaments, where few-cycle field transients are generated as a part of an ultrafast strongly coupled spatiotemporal dynamics, which stretches these transients within extremely short propagation paths, attosecond optical shock waves demonstrated in this work are generated with loosely focused beams, at low gas pressures, and in the regime where ionization effects are negligible. Because of all these factors, such waveforms maintain their pulse widths over much longer propagation paths. Specifically, at $p = 0.02$ bar, the 0.46-fs field waveform shown in Fig. 4(d) remains shorter than 0.65 fs within a propagation path of 70 cm, allowing this field waveform to be extracted from a gas medium with an appropriate pressure gradient, thus making it suitable as a subfemtosecond probe for time-resolved experiments.

In summary, unlike 1D shock waves in optical fibers, 3D shock transients can evolve toward remarkably short, subfemtosecond optical waveforms, suggesting a pulse self-compression scenario whereby multigigawatt attosecond optical waveforms can be synthesized.

This work was supported in part by the Welch Foundation (Grant No. A-1801), the Russian Foundation for Basic Research, and Skolkovo Foundation (Grant No. 78).

[1] A. Toepler, Ann. Phys. (Berlin) **201**, 469 (1865).
[2] E. Mach and L. Sommer, Sitz.ber. Kaiser. Akad. Wiss. Wien **75**, 101 (1877).
[3] L. D. Landau and E. M. Lifshitz, *Fluid Mechanics* (Pergamon, Oxford, 1959), 1st ed.
[4] P. O. K. Krehl, *History of Shock Waves, Explosions and Impact: A Chronological and Biographical Reference* (Springer, Berlin, 2009).
[5] L. A. Ostrovskii, Sov. Phys. JETP **24**, 797 (1967).
[6] D. Grischkowsky, E. Courtens, and J. A. Armstrong, Phys. Rev. Lett. **31**, 422 (1973).
[7] R. L. Fork, C. V. Shank, C. Hirlimann, R. Yen, and W. J. Tomlinson, Opt. Lett. **8**, 1 (1983).
[8] G. Yang and Y. R. Shen, Opt. Lett. **9**, 510 (1984).
[9] J. M. Dudley and S. Coen, Rev. Mod. Phys. **78**, 1135 (2006).
[10] A. M. Zheltikov, Sov. Phys. Usp. **49**, 605 (2006).
[11] L. Bergé, S. Skupin, R. Nuter, J. Kasparian, and J.-P. Wolf, Rep. Prog. Phys. **70**, 1633 (2007).
[12] A. Couairon and A. Mysyrowicz, Phys. Rep. **441**, 47 (2007).
[13] E. E. Serebryannikov, E. Goulielmakis, and A. M. Zheltikov, New J. Phys. **10**, 093001 (2008).
[14] E. Goulielmakis, S. Koehler, B. Reiter, M. Schultze, A. J. Verhoef, E. E. Serebryannikov, A. M. Zheltikov, and F. Krausz, Opt. Lett. **33**, 1407 (2008).
[15] G. P. Agrawal, *Nonlinear Fiber Optics* (Academic, San Diego, 2001).
[16] G. Ben-Dor, O. Igra, and T. Elperin, *Handbook of Shock Waves* (Academic, San Diego, 2000), Vol. 1.
[17] F. DeMartini, C. Townes, T. Gustafson, and P. Kelley, Phys. Rev. **164**, 312 (1967).
[18] D. Anderson and M. Lisak, Phys. Rev. A **27**, 1393 (1983).
[19] K. J. Blow and D. Wood, IEEE J. Quantum Electron. **25**, 2665 (1989).
[20] T. Brabec and F. Krausz, Phys. Rev. Lett. **78**, 3282 (1997).
[21] R. A. Fisher and W. K. Bischel, J. Appl. Phys. **46**, 4921 (1975).
[22] M. Guizar-Sicairos and J. C. Gutiérrez-Vega, J. Opt. Soc. Am. A **21**, 53 (2004).
[23] L. L. Boyle, J. Chem. Phys. **45**, 1318 (1966).
[24] D. M. Bishop and B. Lam, Phys. Rev. A **37**, 464 (1988).
[25] W.-C. Liu, Phys. Rev. A **56**, 4938 (1997).
[26] H. J. Lehmeier, W. Leupacher, and A. Penzkofer, Opt. Commun. **56**, 67 (1985).
[27] M. Masili and A. F. Starace, Phys. Rev. A **68**, 012508 (2003).
[28] L. Brillouin, *Wave Propagation and Group Velocity* (Academic, New York, 1960).